Porphyrin Nanorods

Alexander D. Schwab,[†,‡] Deirdre E. Smith,[‡] Collin S. Rich,[†] Elizabeth R. Young,[‡] Walter F. Smith,*[,†] and Julio C. de Paula*[,‡]

Departments of Physics and Chemistry, Haverford College, 370 Lancaster Avenue, Haverford, Pennsylvania 19041

Received: June 4, 2003; In Final Form: July 29, 2003

Aggregates of the diacid form of tetrakis(4-sulfonatophenyl)porphine (TPPS), formed in acidic aqueous solutions, were deposited onto hydrophilic (mica) and hydrophobic (polystyrene and graphite) substrates and imaged using atomic force microscopy (AFM). The AFM images revealed the aggregates were either individual rods with a diameter of 3.8 ± 0.3 nm and a length of 0.77 ± 0.43 μm or larger structures composed of bundles of individual rods. This study demonstrates that aggregates of the diacid form of TPPS are remarkably straight nanorods with a well-defined height. UV/vis spectroscopy and dynamic light-scattering measurements show that the aggregates form in solution and not on the surface of the substrate, with nucleation of the aggregates being the rate-limiting step, followed by rapid growth at the ends of the rods.

I. Introduction

In photosynthetic light-harvesting complexes, biopolymer scaffolds hold pigments at short enough intermolecular distances that electronic coupling, photon capture, and energy transfer are optimized.[1] An example is the chlorosome, a light-harvesting apparatus that binds to the cytoplasmic side of the cytoplasmic membrane of green photosynthetic bacteria. The chlorosomes of *Chloroflexus aurantiacus* are lipid-rich envelopes measuring 166 ± 37 nm in length, 97 ± 25 nm in width, 24 ± 5 nm in height and containing nearly 200 000 bacteriochlorophyll *c* molecules organized as rod-shaped aggregates, each with a diameter of 5.2 nm.[2,3]

Synthetic tetrapyrrole macrocycles are appropriate mimics of chlorophylls, so the design of artificial light-harvesting systems inspired by the architecture of the chlorosome has been based on self-assembly of aggregates of porphyrins and chlorins either in solution[4] or onto polymer templates.[5,6] Self-assembled porphyrin aggregates in solution, the main subject of this report, have been studied by a variety of crystallographic and microscopic techniques. Kosal and Suslick[7] described a number of microporous materials based on self-association of porphyrins in the solid state. Fuhrhop and co-workers[8] have used scanning tunneling microscopy to image aggregates of hydrophobic *meso*-tetrakis(3,5-dicarboxyphenyl)porphyrin deposited on carbon surfaces. They observed the formation of flat, crystalline layers of the porphyrin on graphite, but not on amorphous carbon films. De Schryver and co-workers[9] have shown by confocal fluorescence microscopy, atomic force microscopy (AFM), and near-field scanning optical microscopy that aggregates of the hydrophobic porphyrin bis(21*H*,23*H*-5(4-pyridyl)-10,15,20-tris-(4-hexadecyloxyphenyl)porphyrin)platinum dichloride evaporated on glass are rings with diameters ranging from 10 nm to several micrometers and heights of 10−200 nm. Udal'tsov et al.[10] evaporated onto glass plates a sample of hydrophobic *meso*-tetraphenylporphine aggregated in tetrahydrofuran−water solution. Analysis by scanning electron microscopy revealed several aggregate geometries, ranging from roughly spherical and ellipsoidal to highly irregular structures with dimensions in the micrometer scale.

Drain and co-workers[11] have shown recently that columnar aggregates of porphyrins can form on surfaces. Their design consisted of assembling a flat nonamer building block held together by coordination of Pd^{2+} ions to peripheral substituents on the porphyrin monomer. AFM measurements showed that the flat units stack on mica and glass, forming columns with heights of 2−6 nm on glass and about 3 nm on mica. Columnar structures did not form on a Au(111) surface. These studies demonstrate important ways in which the shape and size of porphyrin aggregates can be controlled.

The J-aggregates of **2** have been extensively studied using UV/vis spectroscopy[12−15] and various light-scattering techniques.[16,17] The UV/vis studies show that in aqueous solution at pH 7 only **1** is found and at pH 3 only **2** is found. Further increasing the solution electrolyte concentration either through the addition of acid or some other salt, both **2** and its J-aggregate are found in solution. The three porphyrin states, free-base, diacid, and J-aggregate, exhibit absorbance maxima at 413, 435, and 492 nm, respectively.

Three different types of light-scattering measurements have been applied to the study of $H_4TPPS_4^{2-}$ aggregates: elastic light-scattering (ELS), resonance light-scattering (RLS), and dynamic light-scattering (DLS) measurements. ELS measurements, an ambiguous measure of particle size and shape in solution, indicate the presence of cylindrical rodlike aggregates with lengths of 0.6−0.9 μm for acid-induced aggregates prepared from solutions with $[H_4TPPS_4^{2-}] = 2.3-3.7$ μM.[16b] Depolarized DLS measurements in the same study indicate that the most likely rod diameter was 70 nm. Furthermore, RLS measurements suggest that each aggregates has, on average, 3×10^5 to 5×10^5 $H_4TPPS_4^{2-}$ molecules when acid induced aggregates are prepared with $[H_4TPPS_4^{2-}] = 2.3-3.7$ μM.[16b] Later studies by Micali and co-workers, however, employing ELS and DLS led to the conclusion that the acid induced $H_4TPPS_4^{2-}$ aggregates ($[H_4TPPS_4^{2-}] = 5$ μM) are fractal objects with a fractal

* Corresponding authors. E-mail addresses: (W.F.S.) wsmith@haverford.edu; (J.C.d.P.) jdepaula@haverford.edu.
† Department of Physics, Haverford College.
‡ Department of Chemistry, Haverford College.

10.1021/jp035569b CCC: $25.00
Published on Web 09/18/2003

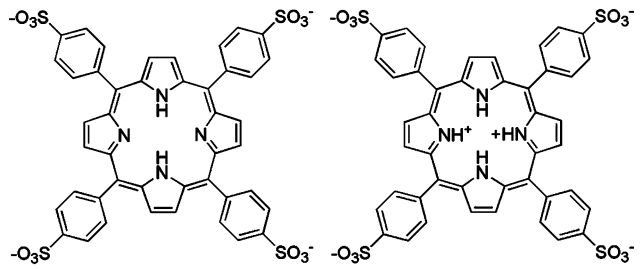

1 $H_2TPPS_4^{4-}$ (pH > 4.8)[12] **2** $H_4TPPS_4^{2-}$ (pH < 4.8)[12]

Figure 1. Structures of the free-base ($H_2TPPS_4^{4-}$, **1**) and diacid ($H_4TPPS_4^{2-}$, **2**) forms of tetrakis(4-sulfonatophenyl)porphine used in this study.

dimension of 1.7 composed of small groups of 6−32 porphyrin molecules.[17]

In this report, we demonstrate that the diacid form of the synthetic porphyrin tetrakis(4-sulfonatophenyl)porphine (Figure 1) self-assembles into rod-shaped J-aggregates in aqueous solutions containing an electrolyte without the need of an assembly template or scaffold. This situation is unlike that found in recent studies of J-aggregates of **2** grown on polylysine scaffolds.[6] The uniformity and straightness of the nanorods we report here were not predicted by solution light-scattering studies or previous transmission electron micrographs of J-aggregates of **2** formed by addition of K^+ salts.[18] Furthermore, the aggregates in our study can easily be deposited onto substrates with a wide-range of hydrophobicities, and the density of aggregates deposited onto a substrate can be controlled by variation of the immersion time of the substrates in the aggregate solution.

II. Experimental Methods

A. Preparation of Aggregate Solutions. The chloride salt of **2** was purchased from Frontier Scientific, Inc. and used as received. Concentrated stock solutions (0.7−1.5 mM) containing both **1** and **2** were first prepared by dissolving the chloride salt of **2** in a 0.1 mM phosphate buffer solution (pH = 6.8). The porphyrin concentration of the stock solution was determined by measuring the absorbance of the Soret band for **1** at 413 nm ($\epsilon_{413} = 5.33 \times 10^5$ M^{-1} cm^{-1})[12] from an aliquot of the stock solution diluted 1/400 by volume with 0.1 mM phosphate buffer. With the porphyrin concentration known, small aliquots of the stock solution were sufficiently diluted with 0.1 mM phosphate buffer to yield solutions of $[H_2TPPS_4^{4-}] = 10$ μM. Though the starting material was the diacid form of the porphyrin, **2**, the buffering capacity of the 0.1 mM phosphate in solution is sufficient to convert **2** to the free-base form, **1**, at low porphyrin concentrations (i.e., <30 μM).

Acid-induced aggregate solutions were made by adding a portion of the $[H_2TPPS_4^{4-}] = 10$ μM solution described in the previous paragraph to an equal volume of 0.6 M HCl and then mixing. This procedure yields a final solution with [HCl] = 0.3 M and $[H_2TPPS_4^{4-}] = 5$ μM (pH = 0.9). The kinetics of aggregation were tracked by monitoring the absorbance of the J-aggregate Soret band at 492 nm.[15] These measurements and additional dynamic light-scattering measurements indicate that the aggregation process is at least 90% complete within an aging time of 1 h. The aging time is defined as the time interval between making the acidified porphyrin solution and immersing the substrate into this solution.

Salt-induced aggregates were prepared by first making a solution of $[H_2TPPS_4^{4-}] = 5$ μM in 0.4 mM HCl (pH = 3.4) and then adding a sufficient quantity of a concentrated salt solution ([NaCl] = 2.5 M in 0.1 mM phosphate buffer) to yield a final solution with [NaCl] = 0.3 M. All aqueous solutions in this study were made using deionized water (18.2 MΩ cm) prepared with a Millipore Simplicity 185 purification apparatus.

B. UV/Vis Measurements. A majority of the UV/vis absorbance measurements were obtained using a Jasco V-570 UV/vis spectrophotometer with the ETC-505T temperature control attachment capable of maintaining temperatures with ±0.1 °C accuracy. To acquire rapid kinetic UV/vis spectra, an Ocean Optics USB2000 UV/vis photodiode array spectrometer was employed which has the capability of acquiring absorbance spectra in a fraction of a second. Poly(methyl methacrylate) cuvettes with a 1 cm path length were used for all absorbance measurements, and a cuvette containing only 0.1 mM phosphate buffer solution was used as the reference. UV/vis absorbance and transmission spectra of material on glass substrates were acquired in a transmission geometry using a clean glass substrate as the reference.

C. Dynamic Light-Scattering Studies. All dynamic light-scattering (DLS) measurements were performed using a Protein Solutions MS/X instrument which includes an 825.2 nm diode laser light source and measures light scattered at an angle of 90°. To verify the presence of aggregates in solution, a 15 μL scattering cell was employed. The DLS measurements of aggregation kinetics, on the other hand, were performed using a standard 1 cm cuvette which allows a sufficiently large volume for proper mixing of the components. The intensity autocorrelation function decay times were calculated using the regularization algorithm (set to "Optimal Resolution") included in the Dynamics V6 software packaged with the DLS instrument.[19]

D. Imaging Studies. Mica and graphite substrates purchased from Novascan Technologies and Structure Probe, Inc., respectively were cleaved immediately before aggregate deposition. Glass substrates cut from microscope slides were soaked in a saturated KOH/alcohol solution for at least 12 h, rinsed in deionized water, and dried with compressed air shortly before use. Polystyrene (PS) (Polymer Source, Inc.) substrates were made by spin coating a 5 wt % solution of PS ($M_w = 2.2 \times 10^5$ g mol^{-1}, $M_w/M_n = 1.03$) in toluene (Aldrich, HPLC grade) at 2000 rpm onto cleaned glass substrates. The substrates were then vacuum annealed at 110 °C for at least 2 h, yielding smooth PS films with a thickness of 312 ± 15 nm. Film thickness was determined by first obtaining a transmission spectrum (350−1000 nm) through the PS film and glass substrate and then comparing wavelengths of transmission maxima and minima to theoretically predicted values.[20]

The deposition of $H_4TPPS_4^{2-}$ aggregates involved placing a small amount onto the substrate or immersing the substrate into the aggregate solution for a specified time. To remove excess solution from the substrate surface after the specified time, the substrate was spun at 4000 rpm for 40 s. The aggregate-coated substrates were then used for absorbance measurements or AFM imaging. All AFM images were obtained with a Digital Instruments Bioscope operated in tapping mode, using standard etched silicon tips (Nanodevices).

III. Results and Discussion

A. UV/Vis Studies of Aggregates. Previous studies on the aggregation kinetics of acid-induced aggregates prepared as described in the Experimental Methods section indicate that the absorbance at 492 nm increases at the expense of the absorbance at 435 nm as the aggregation proceeds.[15] A more detailed investigation of this phenomenon is presented in Figure 2.

It can be seen from Figure 2 that, after an initial induction period of ∼4 min, the peak at 492 nm associated with the

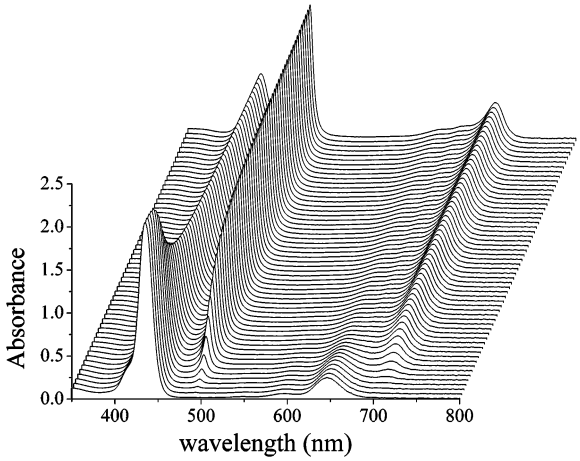

Figure 2. UV/vis spectra acquired during the acid-induced aggregation of $H_4TPPS_4^{2-}$. The foremost spectrum was acquired 50 s after the solution of 10 μM $H_2TPPS_4^{4-}$ was mixed with an equal volume of 0.6 M HCl. All successive spectra were acquired at 1 min intervals as aggregation proceeded. Absorbance peaks at 492 and 705 nm correspond to $H_4TPPS_4^{2-}$ aggregates whereas peaks at 435 and 645 nm are attributed to the free diacid $H_4TPPS_4^{2-}$.

aggregates of **2** begins to increase whereas the peak at 435 nm normally associated with the dimeric form of **2** begins to decrease. After roughly 30 min the aggregation process approaches completion, with the diacid and its aggregate coexisting in solution. The magnitude of the red-shift of the aggregate peak with respect to the diacid absorbance peak is determined by the size of the aggregate based on exciton coupling theory. However, the magnitude of the red-shift ceases to change when the number of molecules in an aggregate becomes larger than 10−20, depending on the packing geometry.[21] The absence of significant absorbance between 435 and 492 nm in Figure 2 therefore indicates the absence of aggregates of this intermediate size. The presence of the kinetic induction period and the lack of small aggregates indicate that the porphyrin aggregates grow by a process in which slow nucleation is followed by fast aggregate growth. In fact, an autocatalytic model where nucleation is the rate-limiting step has been successfully employed to describe $H_4TPPS_4^{2-}$ aggregation kinetics.[15,22]

B. DLS Studies of Aggregation Kinetics. We have followed the growth of $H_4TPPS_4^{2-}$ aggregates by DLS. Intensity autocorrelation data were acquired from aggregating solutions at 1 min intervals after the porphyrin was added to the acid solution at $t = 0$. The scattered intensity as a function of time is shown in Figure 3.

The intensity autocorrelation function can yield information regarding the translational dynamics of molecules in solution. Each mode of motion in an ensemble of molecules has a characteristic decay rate, Γ, and the autocorrelation data can be fit with a summation of Γ_i values. The mathematical form for the resulting intensity autocorrelation function, $g^{(2)}(\tau)$, is given by

$$g^{(2)}(\tau) = 1 + \beta[\sum_i A_i \exp(-\Gamma_i \tau)]^2 \qquad (1)$$

where β is a parameter that depends on the perfection of the experimental system and A_i is the relative amplitude for the dynamic mode corresponding to Γ_i.[19,23] The fit of the autocorrelation data with eq 1 leads to the decay rates shown in Figure 4.

Assuming that each Γ_i corresponds to a translational diffusion mode, it is, in theory, possible to determine the size of the

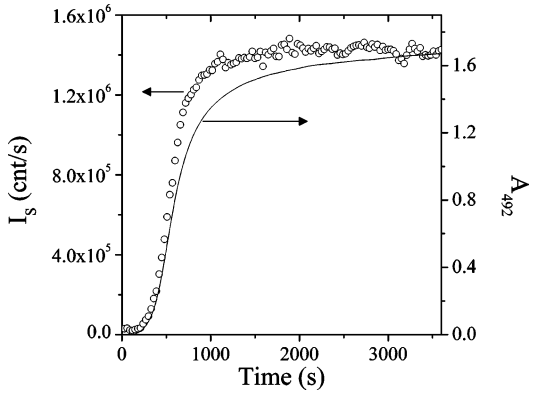

Figure 3. Scattered intensity (I_S) from aggregating solutions of $[H_4TPPS_4^{2-}] = 5$ μM and [HCl] = 0.3 M compared to the absorbance at 492 nm (A_{492}) corresponding to the aggregate absorption peak.

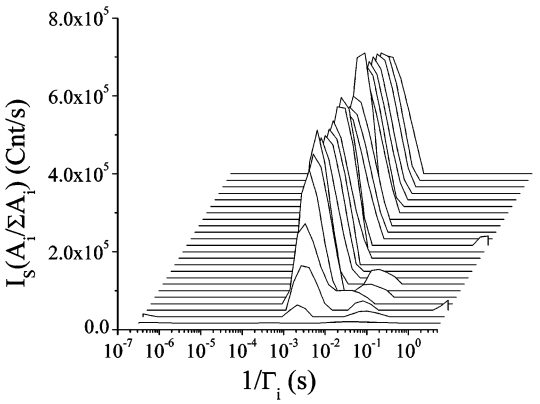

Figure 4. DLS Intensity autocorrelation relative decay amplitudes (A_i) and rates (Γ_i) from aggregating solutions of $[H_4TPPS_4^{2-}] = 5$ μM in 0.3 M HCl. The foremost curve is acquired immediately after the solution is made and each successive curve represents 2.5 ± 0.5 min in time.

aggregates if the aggregate shape is well defined. In the next section, it will be shown that the aggregate dimensions vary, making direct determination of the aggregate size from the data in Figure 4 very problematic. A few statements can, however, be made about the species in the aggregating solutions. First of all, there appears to be one dominant component that increases in number as the aggregation proceeds. This shows that the aggregates do not increase in size as aggregation proceeds, but rather the number of aggregates increases with time. This growth mechanism agrees well with the aforementioned autocatalytic growth mechanism proposed for the $H_4TPPS_4^{2-}$ aggregates.[15]

C. AFM Studies of $H_4TPPS_4^{2-}$ Aggregates. $H_4TPPS_4^{2-}$ aggregates were deposited onto mica substrates, dried, and then imaged with an atomic force microscope (AFM). AFM images of the substrate-deposited aggregates reveal the remarkable aggregate morphologies shown in Figure 5: individual rods and bundles of rods. As demonstrated in the following sections, the single aggregate rods have a remarkably uniform height and these rods appear to be the basic building blocks for larger, bundled aggregates.[24]

The effects of the substrate immersion time on the resulting aggregate morphologies are best illustrated in Figure 6. All three images show the familiar individual rods and rod bundles, but there is an obvious increase in the density of aggregates on the surface with increasing immersion time.

In addition to the characterization of aggregates on mica using AFM, a UV/vis spectrum (in transmission mode) was obtained from aggregates deposited onto a glass substrate as shown in

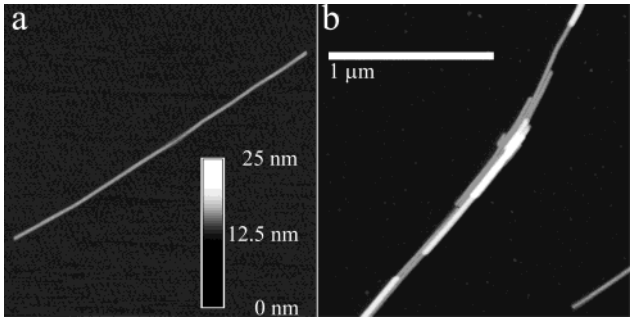

Figure 5. Illustration of the two main structures observed for $H_4TPPS_4^{2-}$ aggregates. (a) AFM image of a single $H_4TPPS_4^{2-}$ rod obtained from a mica substrate immersed 30 s in a 5 μM $H_4TPPS_4^{2-}$, 0.3 M HCl solution aged for 2 h. The aging time of an aggregate solution describes the length of time between the between aggregate solution creation and its use for substrate deposition. (b) AFM image of a $H_4TPPS_4^{2-}$ rod bundle obtained from a mica substrate immersed for 1 h in a 5 μM $H_4TPPS_4^{2-}$, 0.3 M HCl solution aged for 2 h. The lateral and height scales are the same for both images.

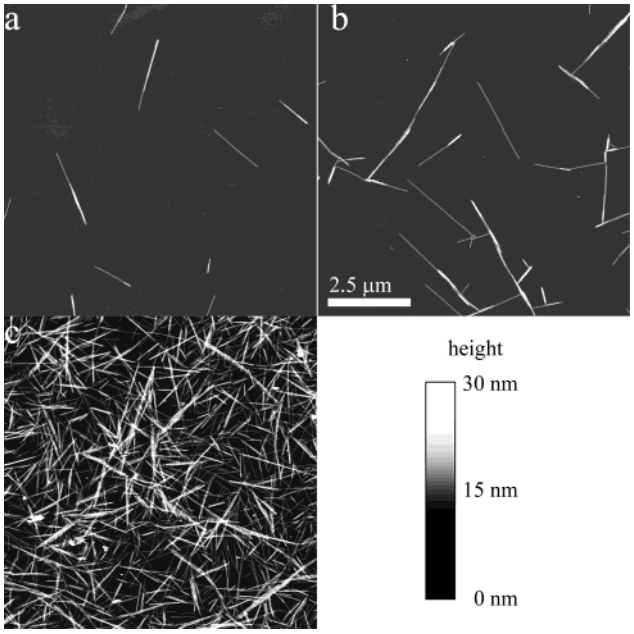

Figure 6. AFM images illustrating the morphologies adopted by $H_4TPPS_4^{2-}$ aggregates as well as the effect that the substrate immersion time has on the surface coverage of $H_4TPPS_4^{2-}$ aggregates. Images were obtained from mica substrates immersed in a 5 μM solution of $H_4TPPS_4^{2-}$ in 0.3 M HCl aged for 2 h. The immersion times were (a) 60 s, (b) 1 h, and (c) 5 days. The lateral and height scales are the same for all three images.

Figure 7. The spectrum of deposited aggregates appears very similar to that of the $H_4TPPS_4^{2-}$ aggregates in solution also shown in Figure 7. The deposited aggregate peaks are seen at 491 and 700 nm with an additional peak appearing at 422 nm which has been assigned to an aggregate H-band in a previous study.[14a] In addition to the peak at 422 nm, there is a broad absorbance feature between 422 and 491 nm that can be attributed to $H_4TPPS_4^{2-}$ monomer or smaller aggregates.

To investigate further the origin of the rodlike features, a number of different protocols were used to deposit aggregates onto mica substrates from 5 μM solutions of **2** in 0.3 M HCl. Because of the irregular shape of the rod bundles, only the dimensions of the individual, nonbundled single rods could be characterized properly by AFM. Care was taken to ensure the density of rods on a substrate was low enough to distinguish individual rod aggregates. As a result, the deposition protocols

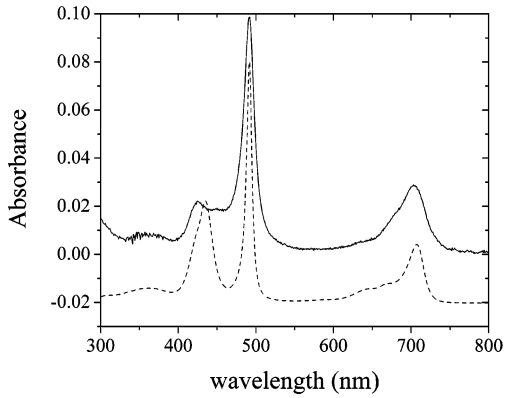

Figure 7. UV/vis absorbance spectrum taken in transmission through a glass substrates immersed for 1077 min in a solution of 5 μM $H_4TPPS_4^{2-}$ in 0.3 M HCl aged 1 h compared to the absorbance spectrum from the deposition solution (dashed line). The solution UV/vis spectrum has been scaled by a factor of 10 and vertically offset for clarity.

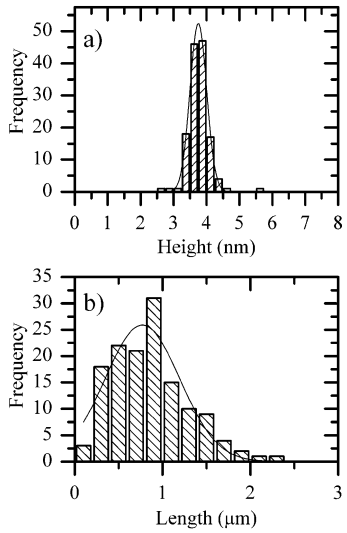

Figure 8. Distributions of rod heights and lengths obtained from AFM images of more than 130 individual rods deposited onto mica substrates from 5 μM $H_4TPPS_4^{2-}$, 0.3 M HCl solutions under various conditions. (a) Distribution of rod heights of individual rods in AFM images. The solid line represents a fit of the data to a Gaussian distribution with a mean of 3.8 nm and a standard deviation of 0.3 nm. (b) Distribution of rod lengths determined from the in-plane end-to-end distance of individual rods appearing in AFM images. The solid line represents a fit of the data to a Gaussian distribution with a mean of 0.77 μm and a standard deviation of 0.43 μm.

involved variations of the immersion time (up to 2 h) as well as different aging times (up to 5 days) for the $H_4TPPS_4^{2-}$ aggregate solutions. The height and in-plane lengths of all distinguishable single rods were recorded from multiple AFM images from multiple samples. Analysis of more than 130 individual rods deposited by a wide variety of protocols shows that single rods form with a narrow distribution of heights with an average of 3.8 nm and a standard deviation of 0.3 nm, as illustrated in Figure 8. The narrowness of the height distribution is remarkable considering the standard deviation of the height for a cleaved mica surface is 0.2 nm. Furthermore, the persistent dimension of 3.8 nm was found regardless of the aggregate deposition conditions.

As also summarized in Figure 8, the lengths of the single rods were found to vary from 130 nm to 2.3 μm with no apparent correlation between the immersion (up to 2 h) or aging times (up to 5 days each) and the length. Parts b and c of Figure

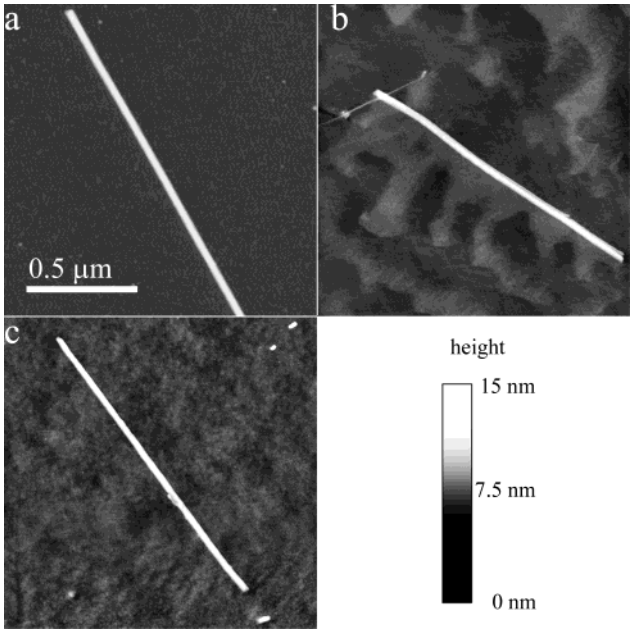

Figure 9. AFM images of $H_4TPPS_4^{2-}$ aggregates deposited onto (a) mica, (b) graphite, and (c) polystyrene substrates. Deposition solution was 5 μM $H_4TPPS_4^{2-}$ and 0.3 M HCl aged for 2 h, and the immersion time was 30 s.

6, and additional images not shown, indicate that the bundles of rods can be up to 5 μm in length and 40 nm in diameter.

The sizes of the individual rods characterized with AFM differ from what was expected based on solution light-scattering measurements. The rod heights in Figure 8, 3.8 ± 0.3 nm, are much smaller and more uniform than those indicated from previous light-scattering measurements.[16] The difference is best explained by the more intense scattering from the larger, bundled rod aggregates in solution. Consequently, the light-scattering measurements appear to report primarily on the size of the rod bundles we observed with AFM.

D. Effects of Substrate Hydrophobicity. To test the effect of substrate hydrophobicity on the aggregates, we used three different substrates, mica, graphite, and polystyrene (PS) (listed in order of increasing hydrophobicity).[25−27] As seen in Figure 9, aggregates of the same size and shape were deposited onto all three substrates despite their widely varied hydrophobicities. Additional images, not shown, also indicate that the substrate hydrophobicity has no effect on promotion or prevention of aggregate growth or deposition. Furthermore, control experiments demonstrated that aggregates are only observed by AFM when they are also present in solution as judged by DLS and UV/vis spectroscopy. For example, deposition of solutions of **1** at pH 7 and **2** at pH 3 onto mica did not lead to rodlike structures as imaged by AFM. These observations, especially when combined with the findings of the solution-based studies, indicate that the growth of the nanorods is not catalyzed by the surface. Additionally, we suggest that the lengths of the aggregates (the nanorods) are controlled by their mechanical stability in solution, which also determines their fate during solution deposition and the handling of the wet substrates.

E. Salt-Induced Aggregates. Several studies have already shown that it is possible to induce the aggregation of **2** with a nonacidic electrolyte.[13−15,17a] To make salt-induced aggregates, a concentrated salt solution was added to a 5 μM $H_4TPPS_4^{2-}$ solution (pH = 3.4). These salt-induced aggregates were then deposited onto mica substrates and imaged using AFM. The morphology adopted by the salt-induced aggregates is shown

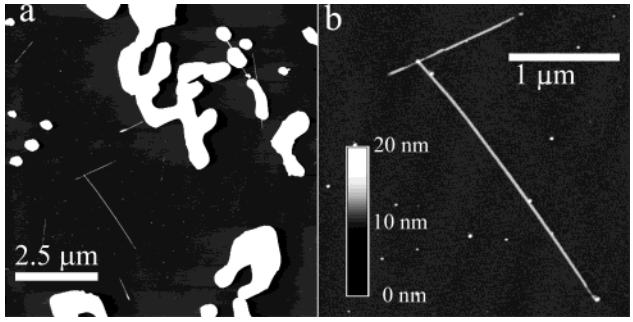

Figure 10. AFM Image of salt-induced aggregates deposited onto mica substrates from a solution of 5 μM $H_4TPPS_4^{2-}$, 0.4 mM HCl, and 0.3 M NaCl aged for 2 h. (a) A 10 × 10 μm image of $H_4TPPS_4^{2-}$ aggregates and NaCl crystals. Control experiments verified the large, rounded objects in the image were due to NaCl. (b) A 3 × 3 μm image of $H_4TPPS_4^{2-}$ aggregates. Immersion time was 30 s. Both images share the same vertical height scale.

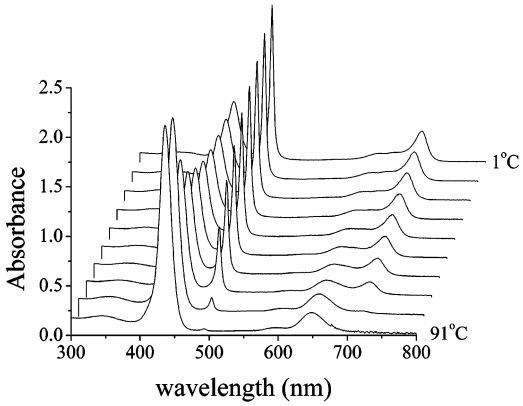

Figure 11. UV/vis absorption spectra of a 5 μM $H_4TPPS_4^{2-}$, 0.3 M HCl solution taken at different temperatures. The foremost spectrum was taken at 91 °C, and each successive spectrum was taken in 10 °C increments as the solution was cooled from 91 °C to 1 °C. Spectra were acquired at 10 °C intervals after equilibrating for 1 h at each temperature.

in Figure 10. Objects with two different shapes appear in the image: tall (>100 nm), rounded objects and lower, rod-shaped objects. Images of samples prepared from a control solution consisting of 0.3 M NaCl, 0.1 mM phosphate buffer, and 0.4 mM HCl, but containing no porphyrin, show that the tall, round objects appearing in Figure 10 are salt crystals. The remaining rod-shaped objects have the same diameter (height = 3.9 nm) and lengths as the acid-induced aggregates.

F. Control of Aggregate Size. The fact that aggregates of $H_4TPPS_4^{2-}$ can be induced by the addition of a wide variety of ions dissolved in aqueous solution suggests a solubility model for that aggregation. By increasing the ionic strength of the aqueous solution, the solution's ability to solvate the zwitterionic $H_4TPPS_4^{2-}$ species is reduced. At that point, the $H_4TPPS_4^{2-}$ molecules are forced to leave the solution and do so by assembling into the rod-shaped aggregates. If this explanation is correct, then it should be possible to push the $H_4TPPS_4^{2-}$ monomer−aggregate equilibrium toward monomer formation by increasing the temperature. This is exactly the behavior shown in Figure 11. At 91 °C, the solution is composed almost entirely of the nonaggregated diacid (peaks at 435 and 645 nm) whereas at lower temperatures more of the aggregate appears (peaks at 492 and 705 nm).

Having shown that the solubility limit of $H_4TPPS_4^{2-}$ can be controlled by temperature, it should be possible to manipulate the dimensions of the aggregates by employing techniques analogous to those used to grow single crystals from aqueous

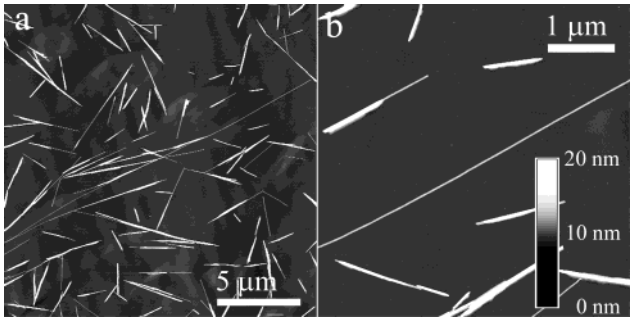

Figure 12. AFM images from mica substrates immersed in a 5 μM $H_4TPPS_4^{2-}$, 0.3 M HCl solution as it was cooled at a rate of 0.5 °C min^{-1} from 95 to 60 °C. (a) A 20 × 20 μm image showing some single rods that are longer than 20 μm in length. (b) A 5 × 5 μm image showing a 5.6 μm long continuous segment of a single rod aggregate.

solution.[28] A solution was first heated to a temperature where no aggregates appear in solution (95 °C) as determined by UV/vis spectroscopy. A mica sheet was inserted into the solution and then the solution was slowly cooled at a rate of 0.5 °C min^{-1}. At some temperature, nucleating species began to form. If we assume that aggregate growth is easier than aggregate nucleation, the existing aggregates should continue to grow as the temperature of the solution is slowly lowered. Since we have established that the individual rod aggregates all have a single diameter, growth of the aggregates must occur at the rod ends leading to aggregates that are longer than those obtained by aggregating at room temperature.

Figure 12 shows AFM images obtained from a mica substrate immersed in a $H_4TPPS_4^{2-}$ solution that was cooled at a rate of 0.5 °C/min from 95 to 60 °C. In Figure 12a, it appears as if some of the aggregates may be over 20 μm long with Figure 12b showing a 5.6 μm long continuous section of a rod-shaped aggregate. Though the slow-cooling methods described here can be used to generate long porphyrin nanorods, it does not provide absolute control of aggregate length. We are currently working on alternative strategies that may allow us to tune nanorod length more finely.

IV. Conclusions

Increasing the ionic strength of aqueous solutions of $H_4TPPS_4^{2-}$ leads to the formation of either single rod-shaped aggregates with a height of 3.8 ± 0.3 nm or bundles of these same rods. The height of the single porphyrin nanorods persisted over a broad range of experimental deposition conditions. The uniformity of height makes these structures useful as nanometer-sized building blocks for nanometer-sized structures or as nanometer height calibration standards.

Though some methods were introduced to control the aggregate deposition density and aggregate length, it would also be desirable to control the rod-bundling behavior. The exact mechanism of rod bundling remains unclear, but two possibilities exist. The side of a single aggregate rod in solution may serve as a nucleation site for the growth of another rod, or single rods in solution may bump into one another and "stick" due to an attractive interaction.

The reasons for assembling into a rod shape rather than any other shape are likely due to the specific intermolecular interactions between the individual $H_4TPPS_4^{2-}$ molecules. Exciton coupling theory suggests that since the Soret absorption peak of $H_4TPPS_4^{2-}$ is red shifted upon aggregation (a J-aggregate), the planar porphyrin molecules are stacked in an arrangement where individual porphyrin units are not positioned directly one on top of the other. X-ray scattering measurements are currently underway to determine the packing arrangement of $H_4TPPS_4^{2-}$ molecules in the aggregates. This should help elucidate which intermolecular interactions are important in determining the overall shape of a molecular self-assembled structure.

The electronic coupling present in these aggregates makes them potentially useful for application as nanowires, nanometer-sized photoconductors, or as antennae in synthetic light-harvesting complexes. For example, the light-harvesting apparatus (the chlorosome) of *Chloroflexus aurantiacus* contains nearly 200 000 bacteriochlorophyll *c* molecules organized as rod-shaped aggregates, each with a diameter of 5.2 nm.[2,3] Photoconductivity measurements are currently underway to test this potential ability of the porphyrin nanorods.

Acknowledgment. We acknowledge valuable discussion with Profs. Luigi Monsu-Scolaro, Robert Pasternack, Esther Gibbs, Peter Collings, Karin Åkerfeldt, Robert Fairman, Robert Manning, and Karl Johnson. This work was supported by grants from the David and Lucile Packard Foundation (W.F.S. and J.C.d.P.), the National Science Foundation (CHE-9900403 and DBI-0070361) (J.C.d.P. and W.F.S.), and the Camille and Henry Dreyfus Foundation (J.C.d.P.).

References and Notes

(1) Pullerits, T.; Sundström, V. *Acc. Chem. Res.* **1996**, *29*, 381−389.
(2) Martinez-Planells, A.; Arellano, J. B.; Borrego, C. M.; Lopez-Iglesias, C.; Gich, F.; Garcia-Gil, J. *Photosyn. Res.* **2002**, *71*, 83−90.
(3) Olson, J. M. *Photochem. Photobiol.* **1998**, *67*, 61−75.
(4) Kano, K.; Fukuda, K.; Wakami, H.; Nishiyabu, R.; Pasternack, R. F. *J. Am. Chem. Soc.* **2002**, *122*, 7494−7502.
(5) (a) Pasternack, R. F.; Giannetto, Pagano, P.; Gibbs, E. J. *J. Am. Chem. Soc.* **1991**, *113*, 7799−7800. (b) Pasternack, R. F.; Goldsmith, J. I.; Szép, S.; Gibbs, E. J. *Biophys. J.* **1998**, *75*, 1024−1031.
(6) Koti, A. S. R.; Periasamy, N. *Chem. Mater.* **2003**, *15*, 369−371.
(7) Kosal, M. E.; Suslick, K. S. *J. Solid State Chem.* **2000**, *152*, 87−98.
(8) Li., G.; Fudickar, W.; Skupin, M.; Klyszcz, A.; Draeger, C.; Lauer, M.; Fuhrhop, J.-H. *Angew. Chem., Int. Ed* **2002**, *41*, 1828−1852.
(9) (a) Hofkens, J.; Latterini, L.; Vanoppen, P.; Faes, H.; Jeuris, K.; De Feyter, S.; Kerimo, J.; Barbara, P. F.; De Schryver, F. C.; Rowan, A. E.; Nolte, R. J. M. *J. Phys. Chem. B* **1997**, *101*, 10588−10598. (b) Latterini, L.; Blossey, R.; Hofkens, J.; Vanoppen, P.; De Schryver, F. C.; Rowan, A. E.; Molte, R. J. M. *Langmuir* **1999**, *15*, 3582−3588.
(10) Udal'tsov, A. V.; Kazarin, L. A.; Sinani, V. A.; Sweshnikov, A. A. *J. Photochem. Photobiol. A* **2002**, *151*, 105−119.
(11) Drain, C. M.; Batteas, J. D.; Flynn, G. W.; Milic, T.; Chi, N.; Yabloon, D. G.; Sommers, H. *Proc. Natl. Acad. Sci. U.S.A.* **2002**, *99*, 6498−6502.
(12) Fleischer, E. B.; Palmer, J. M.; Srivastava, T. S.; Chatterjee, A. *J. Am. Chem. Soc.* **1971**, *93*, 3162−3167.
(13) Ohno, O.; Kaisu, Y.; Kobayashi, H. *J. Chem. Phys.* **1993**, *99*, 4128−4139.
(14) (a) Akins, D. L.; Zhu, H.-R.; Guo, C. *J. Phys. Chem.* **1994**, *98*, 3612−3618. (b) Akins, D. L.; Zhu, H.-R.; Guo, C. *J. Phys. Chem.* **1996**, *100*, 5420−5425.
(15) Pasternack, R. F.; Fleming, C.; Herring, S.; Collings, P. J.; de Paula, J.; DeCastro, G.; Gibbs, E. J. *Biophys. J.* **2000**, *79*, 550−560.
(16) (a) Pasternack, R. F.; Schaefer, K. F.; Hambright, P. *Inorg. Chem.* **1994**, *33*, 2062−2065. (b) Collings, P. J.; Gibbs, E. J.; Starr, T. E.; Vafek, O.; Yee, C.; Pomerance, L. A.; Pasternack, R. F. *J. Phys. Chem B* **1999**, *103*, 8474−8481.
(17) (a) Micali, N.; Mallamace, F.; Romeo, A.; Purrello, R.; Monsù Scolaro, L. *J. Phys. Chem. B* **2000**, *104*, 5897−5904. (c) Micali, N.; Romeo, A.; Lauceri, R.; Purrello, R.; Mallamace, F.; Monsù Scolaro, L. *J. Phys. Chem. B* **2000**, *104*, 9416−9420.
(18) Maiti, N. C.; Mazumdar, S.; Periasamy, N. *J. Porphyrins Phthalocyanines* **1998**, *2*, 369−376.
(19) *Dynamics V6*, version 6.3.01; DynaPro dynamic light scattering instrument control software for molecular research. Protein Solutions: Piscataway, NJ, 2002.
(20) Schwab, A. D. Relaxations in Thin Polystyrene Films. Ph.D. Dissertation, The University of Akron, Akron, OH, Dec. 2002.
(21) Parkash, J.; Robblee, J. H.; Agnew, J.; Gibbs, E.; Collings, P.; Pasternack, R. F.; de Paula, J. C. *Biophys. J.* **1998**, *74*, 2089−2099.
(22) Pasternack, R. F.; Gibbs, E. J.; Collings, P. J.; de Paula, J. C.; Turzo, L. C.; Terracina, A. *J. Am. Chem. Soc.* **1998**, *120*, 5873−5878.

(23) Berne, B. J.; Pecora, R. *Dynamic Light Scattering*; Dover Publications: Mineola, NY, 2000.

(24) In a recent report (*Org. Lett.* **2003**, *5*, 1395−1398), Hatano et al. suggest in a footnote that aggregates of **2** prepared in LiCl solution form nanoscale fibers. Their AFM images (see their Supporting Information for their report) do indeed show bundled fibers. However, these fibers are of slightly smaller height (ca. 3 nm) and appear to be less uniform in diameter than the nanorods presented in this paper. We presume the difference is due to the different solution conditions.

(25) Mica was found to be easily wetted with water; the contact angle was too low to be measured readily.

(26) Schrader, M. R. *J. Phys. Chem.* **1975**, *79*, 2508−2515.

(27) Extrand, C. W.; Kumagai, Y. J. *Colloid Interface Sci.* **1997**, *191*, 378−383.

(28) Brice, J. C. In *The Growth of Crystals from Liquids*; Wohlfarth, E. P., Ed.; Selected Topics in Solid State Physics 12; Elsevier/North-Holland: New York, 1973.